



## Chaotic vibrations of flexible infinite length cylindrical panels using the Kirchhoff–Love model

J. Awrejcewicz<sup>a,\*</sup>, V.A. Krysko<sup>b</sup>, V. Nazar'iantz<sup>b</sup>

<sup>a</sup> *Department of Automatics and Biomechanics, Technical University of Lodz, 1115 Stefanowski St., 90-924 Lodz, Poland*

<sup>b</sup> *Department of Mathematics, The Saratov National Technical University, 77 Polytekhnicheskaya St., 410054 Saratov, Russia*

Received 24 August 2004; received in revised form 31 March 2005; accepted 5 April 2005  
Available online 11 July 2005

---

### Abstract

Treated as continuous deformable systems with an infinite number of degrees of freedom, flexible infinite length cylindrical panels subject to harmonic load are studied. Using the finite difference method with respect to spatial coordinates, the continuous system is reduced to lumped one governed by ordinary differential equations. These equations are transformed to a normal form and then solved numerically using the fourth order Runge–Kutta method. In order to trace and explain vibrational behaviour, dependencies  $w_{\max}(q_0)$  and Lyapunov exponents are calculated for panels with parameter value  $k_x = 48$ . The corresponding charts of the control parameters  $\{q_0, \omega_q\}$  are also reported. Novel scenarios yielding chaotic dynamics exhibited by cylindrical panels are illustrated and discussed.

© 2005 Elsevier B.V. All rights reserved.

*PACS:* 02.60.Cb; 02.60.Lj; 02.70.Bf; 05.45.Ac; 46.70.De

*Keywords:* Chaos; Flexible panels; Differential equations; Shells

---

---

\* Corresponding author. Tel.: +48 42 631 23 78; fax: +48 42 631 22 25.  
*E-mail addresses:* [awrejcew@p.lodz.pl](mailto:awrejcew@p.lodz.pl) (J. Awrejcewicz), [tak@san.ru](mailto:tak@san.ru) (V. Nazar'iantz).

## 1. Introduction

Investigations devoted to an analysis of interaction between chaos and order have been carried out recently. They have shown, among others, that a behaviour of complex systems with many degrees of freedom studied in nonlinear non-equilibrium space, where the rules of equilibrium thermodynamics do not work, is characterized by a particular regularity and self-organization.

There exist some regular spatial and temporal structures referred to as Prigogine dissipative systems. Chirikov is one of the first who addressed the problem on chaotic behaviour exhibited by a Hamiltonian system.

An example of a dissipative system with chaotic behaviour has been studied by Lorenz [1], who showed chaos owing to three modes approximation of a two-dimensional problem of heat convection.

Although the chaotic vibrations exhibited by plates and shells have been analysed less, recently it has been developed more intensively.

It is well known that plates (shells) are members of a range of engineering structures (such as building, bridges and tanks) and machines (power plants, flight vehicles, brake systems and mechanical devices), and a full understanding of their dynamics plays a crucial role in development of high technology constructions and mechanics.

Although vibrations of flexible plates of infinite length are considered in a series of publications, in a majority of them a continuous system is analysed as a one-degree-of-freedom system. The method of multiple scales is used by Abe et al. [2] to analyse the two-mode response of simply supported laminated plates subjected to harmonic excitation. The multiple scales technique is applied to analyse sub-harmonic traveling waves of thin, axisymmetric and geometrically nonlinear circular plates [3]. Wei Zhang et al. [4] used the Galerkin method to derive averaged equations from the von Kármán equation, and to analyse both local and global bifurcations of a parametrically and externally excited simply supported rectangular thin plate. Recently, the nonlinear forced vibrations of a thermally loaded annular plate, with clamped boundaries and in the presence of a three-to-one internal resonance between first and second axisymmetric modes has been studied by Arafat and Nayfeh [5].

Various models governing the nonlinear dynamics of plates and shells possess their own history and still require rigorous mathematical treatment. For example, we briefly mention the von Kármán equation considered in Refs. [4,5]. The von Kármán equations are used in Ref. [6] to analyse the nonlinear vibrations of polar orthotropic clamped plates at elevated temperatures. It has been shown, among others, that thermal stresses decrease the vibrations period. In Ref. [7], the von Kármán equations are used to investigate the nonlinear free vibrations of isotropic and polar orthotropic annular plates possessing a rigid mass under action of thermal loads. Finite dimensionality and compactness of attractors for the von Kármán equation are considered by Lasiecka [8]. More generalized questions are also addressed in Refs. [9–11].

Various aspects of the chaotic dynamics of continuous mechanical systems have been studied by the authors of this paper and their coworkers.

Spatio-temporal chaos and solitons exhibited by von Kármán model have been studied in Ref. [12]. An effective algorithm, among others, has been proposed and applied to convert a problem of finding solutions to the hybrid-type partial differential equations (the so-called von Kármán form) to that of ordinary differential and algebraic equations.

Bifurcation and routes to chaos exhibited by a thin plate strips are analysed in Ref. [13]. Jump-like switching phenomena, series of bifurcations, a route to chaos and various types of strange chaotic attractors have been reported and discussed.

A mechanism of transition to chaos of deterministic systems with infinite number of degrees of freedom using the example of parametric vibrations of flexible rectangular plates is reported in paper [14].

Regular and chaotic vibrations and bifurcations of flexible plate strips with non-symmetric boundary conditions are investigated through the Bubnov–Galerkin and finite difference method in Ref. [15]. Some new examples of routes from regular to chaotic dynamics, and within chaotic dynamics have been illustrated and discussed. The phase transitions from chaos to hyper chaos, and a novel phenomenon of a shift from hyper chaos to hyperhyper chaos has also been reported.

Complex vibrations of an Euler–Bernoulli beam with different types of nonlinearities have been considered in Ref. [16]. An arbitrary beam clamping has been considered, and a deflection constraints (point barriers) have been introduced in some beam points along its length. The influence of a constraint as well as the amplitude and frequency of excitation on the vibrations has been analysed. Scenarios of the transition to chaos owing to the nonlinearities have been reported.

This work is focused on an investigation of the chaotic vibrations of long cylindrical panels. In what follows we illustrate and discuss new results associated with a study of spatial–temporal chaos.

## 2. Statement of the problem

Isotropic infinite length shells, i.e., where the shell material satisfies Hook’s law and where a geometrical nonlinearity is taken into account, are studied. To be specific, the coupling between deformations of mean surface and displacements has the form

$$\varepsilon_x = \frac{\partial u}{\partial x} - k_x w + \frac{1}{2} \left( \frac{\partial w}{\partial x} \right)^2. \tag{1}$$

The full deformation of an arbitrary point along a thickness  $\varepsilon_x^z$  is composed of deformations in the mean surface  $\varepsilon_x$  and bending deformations ( $\varepsilon_x^z = \varepsilon_x + \varepsilon_{x,u}$ ), which due to Kirchhoff–Love hypothesis read

$$\varepsilon_{x,u} = -z \frac{\partial^2 w}{\partial x^2}. \tag{2}$$

Consider the shell motion in time interval  $t_0$  and  $t_1$ , and compare the different trajectories of motion of the system of points between initial and final system states. True trajectories are characterized through the following condition:

$$\int_{t_0}^{t_1} (\delta K - \delta \Pi + \delta' W) dt = 0, \tag{3}$$

where  $K$  denotes kinetic energy,  $\Pi$  is potential energy and  $\delta' W$  denotes sum of the elementary works of external forces.

In this case, when all acting forces on the system possess potential, equality (3) takes the form (the Hamilton–Ostrogradsky principle):

$$\delta S = \delta \int_{t_0}^{t_1} (K - \Pi) dt = 0, \tag{4}$$

where  $S = \int_{t_0}^{t_1} (K - \Pi) dt$  is the Hamilton action.

After standard operations and transformations into dimensionless form, the following equations with respect to displacements are derived:

$$\begin{aligned} \frac{\partial^2 u}{\partial x^2} - k_x \frac{\partial w}{\partial x} + \frac{\partial w}{\partial x} \frac{\partial^2 w}{\partial x^2} + p_x - \frac{\partial^2 u}{\partial t^2} = 0, \\ - \frac{1}{12} \frac{\partial^4 w}{\partial x^4} + \frac{\partial w}{\partial x} \left( \frac{\partial^2 u}{\partial x^2} - k_x \frac{\partial w}{\partial x} + \frac{\partial w}{\partial x} \frac{\partial^2 w}{\partial x^2} \right) \\ + \left( k_x + \frac{\partial^2 w}{\partial x^2} \right) \left( \frac{\partial u}{\partial x} - k_x \frac{\partial w}{\partial x} + \frac{1}{2} \left( \frac{\partial w}{\partial x} \right)^2 \right) + q - \frac{1}{12} \frac{\partial^2 w}{\partial t^2} - \varepsilon \frac{\partial w}{\partial t} = 0. \end{aligned} \tag{5}$$

The transformation to non-dimensional form has been realized through relations:

$$\begin{aligned} \bar{k}_x = \frac{a}{R_x} \frac{1}{\lambda}, \quad p_x = \frac{E}{1 - \nu^2} \lambda^3 \bar{p}_x, \quad q = \frac{E}{1 - \nu^2} \lambda^4 \bar{q}, \quad \lambda = \frac{h}{a}, \\ t = a \sqrt{\frac{(1 - \nu^2) \gamma}{Eg}} \bar{t}, \quad u = \bar{u} \lambda^2, \quad x = a \bar{x}, \end{aligned} \tag{6}$$

where bars are associated with dimensionless quantities, and omitted (for simplicity) in Eq. (5). In relations (6)  $E$  is elasticity modulus,  $\nu$  is Poisson’s coefficient,  $\gamma$  denotes the specific gravity of the material,  $g$  is the Earth acceleration,  $q = q(x, t)$  is the transversal load,  $h$  and  $a$  denote thickness and the linear shell dimension,  $w$  and  $u$  are the deflection and displacement of the mean surface, respectively;  $k_x = \frac{1}{R_x}$  is the shell curvature.

The following boundary and initial conditions are attached to Eq. (5).

The boundary conditions read:

1. Ball-type unmovable support

$$u = w = \frac{\partial^2 w}{\partial x^2} = 0, \quad \text{for } x = 0; 1. \tag{7}$$

2. Stiff clamping

$$u = w = \frac{\partial w}{\partial x} = 0, \quad \text{for } x = 0; 1. \tag{8}$$

3. Hybrid type support

$$\begin{aligned} \text{for } x = 0, \quad u = w = \frac{\partial^2 w}{\partial x^2} = 0 \quad \text{ball – type unmovable support;} \\ \text{for } x = 1, \quad u = w = \frac{\partial w}{\partial x} = 0 \quad \text{stiff clamping.} \end{aligned} \tag{9}$$

The initial conditions for  $t = 0$  read:

$$u = f_1(x), \quad \dot{u} = f_2(x), \quad w = f_3(x), \quad \dot{w} = f_4(x). \tag{10}$$

Partial derivatives with respect to  $x$  appeared in (5) are approximated through difference relations with an error of  $O(h_1^4)$  using the Taylor series expansion in vicinity of the point  $x_i$  and with respect to the powers of  $h_1$  ( $h_1$  denotes partition step  $x \in [0,1]$ ):

$$G_{h_1} = \left\{ 0 \leq x_i \leq 1, \quad x_i = ih_1, \quad 0 \leq i \leq N, \quad h_1 = \frac{1}{N} \right\}.$$

In this case, the partial differential equation (5) are transformed to the following second order ordinary differential equations (ODEs) with respect to time for  $i$ th point of the interval  $[0, 1]$ :

$$\begin{aligned} \ddot{u}_i &= A_{x^2}(u_i) - A_x(w_i)(k_x - A_{x^2}(w_i)) + p(ih_1, t), \\ \ddot{w}_i + \varepsilon \dot{w}_i &= \lambda^2 \left( -\frac{1}{12} A_{x^4}(w_i) + A_x(w_i)(A_{x^2}(u_i) - A_x(w_i)(k_x - A_{x^2}(w_i))) \right) \\ &\quad + (A_{x^2}(w_i) + k_x)(A_x(u_i) - k_x w_i + 0.5(A_x(w_i))^2) + q(ih_1, t), \end{aligned} \tag{11}$$

where the difference operators read:

$$\begin{aligned} A_x(\cdot)_i &= \frac{-\cdot_{i+2} + 8\cdot_{i+1} - 8\cdot_{i-1} + \cdot_{i-2}}{12h_1} = \left( \frac{\partial(\cdot)}{\partial x} \right)_i + O(h_1^4), \\ A_{x^2}(\cdot)_i &= \frac{-\cdot_{i+2} + 16\cdot_{i+1} - 30\cdot_i + 16\cdot_{i-1} - \cdot_{i-2}}{12h_1^2} = \left( \frac{\partial^2(\cdot)}{\partial x^2} \right)_i + O(h_1^4), \\ A_{x^4}(\cdot)_i &= \frac{-\cdot_{i+3} + 12\cdot_{i+2} - 39\cdot_{i+1} + 56\cdot_i - 39\cdot_{i-1} + 12\cdot_{i-2} - \cdot_{i-3}}{6h_1^4} \\ &= \left( \frac{\partial^4(\cdot)}{\partial x^4} \right)_i + O(h_1^4). \end{aligned} \tag{12}$$

The boundary and initial conditions are as follows:

Boundary conditions:

1. Ball-type unmovable support

$$u_i = w_i = A_{x^2}(w_i) = 0, \quad i = 0; N. \tag{13}$$

2. Stiff clamping

$$u_i = w_i = A_x(w_i) = 0, \quad i = 0; N. \tag{14}$$

3. Condition (10) is a combination of conditions (13) and (14). Initial conditions:

$$u_i = f_1(ih_1), \quad \dot{u}_i = f_2(ih_1), \quad w_i = f_3(ih_1), \quad \dot{w}_i = f_4(ih_1). \tag{15}$$

The second order ODEs (11) are transformed to first order ODEs, which are then solved using the fourth-order Runge–Kutta method.

### 3. Reliability of the obtained results

The numerical convergence of the numerical solution results with respect to spatial variable  $x$  and time  $t$  has been investigated.

In Table 1 signals  $w(0.5; t)$ , phase portraits  $w(\dot{w})$  and power spectra  $S(\omega)$  for different partition of the spatial variable  $x$  and time under action of transversal load  $q(x, t) = q_0 \sin \omega_q t$  with  $q_0 = 500$  and  $\omega_p = 0.46$  for harmonic bifurcations ( $k_x = 48, \varepsilon = 0.1$ ) are reported.

Analysis of the results shows that in order to get close to exact solutions, it is efficient to consider partition of the interval  $[0, 1]$  with  $N = 16$ . Applying the Runge principle for  $N = 32, 64$  and  $128$ , variations introduced into the signal  $w(0.5, t)$ , phase portrait  $w(\dot{w})$  and power spectrum  $S(\omega)$  are not observed.

Consider the same problem when the construction is within a chaotic state. In Table 2, the same characteristics as in Table 1 are reported (for  $q_0 = 3500$  and  $\omega_p = 0.46$ ).

Observe that although signals for different partitions do not overlap, the integral signal characteristics, i.e., phase portraits and power spectra, are practically the same. Therefore, a number of  $N = 32$  has been used.

In order to detect any particularities of cylindrical panel vibrations, charts of the control parameters  $\{q_0, \omega_p\}$  are constructed (Figs. 1 and 2). They are designed in the light of the power spectrum and largest Lyapunov exponent computations. The full chart is shown in Fig. 1, whereas it's part A is shown in Fig. 2. In order to obtain the chart shown in Fig. 1, the area of control parameters  $\{q_0, \omega_p\}$  has been partitioned into a mesh with steps  $\{4, 0.00115\}$ .

### 4. Lyapunov exponents

Lyapunov exponents play an important role in theory of Hamiltonian and dissipative dynamical systems, because they measure intensity of chaotic behaviour. On the other hand, there is also a link between Lyapunov exponents and other characteristics of chaos, like Kolmogorov's entropy and fractal dimension.

In general, Lyapunov exponents describe an averaged velocity of exponential divergence of close trajectories (see, for example, [13]). A number of the computation of Lyapunov exponents

Table 1  
Signals, phase portraits and power spectra (Section 3;  $q_0 = 500$ )

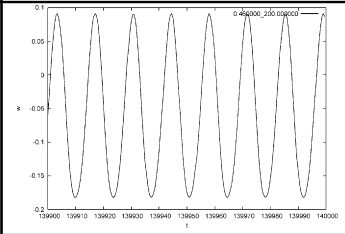
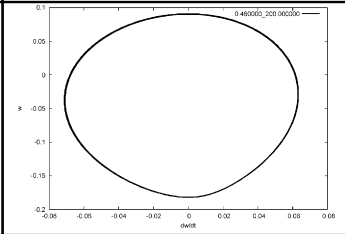
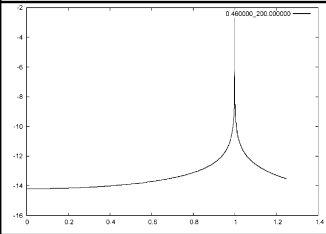
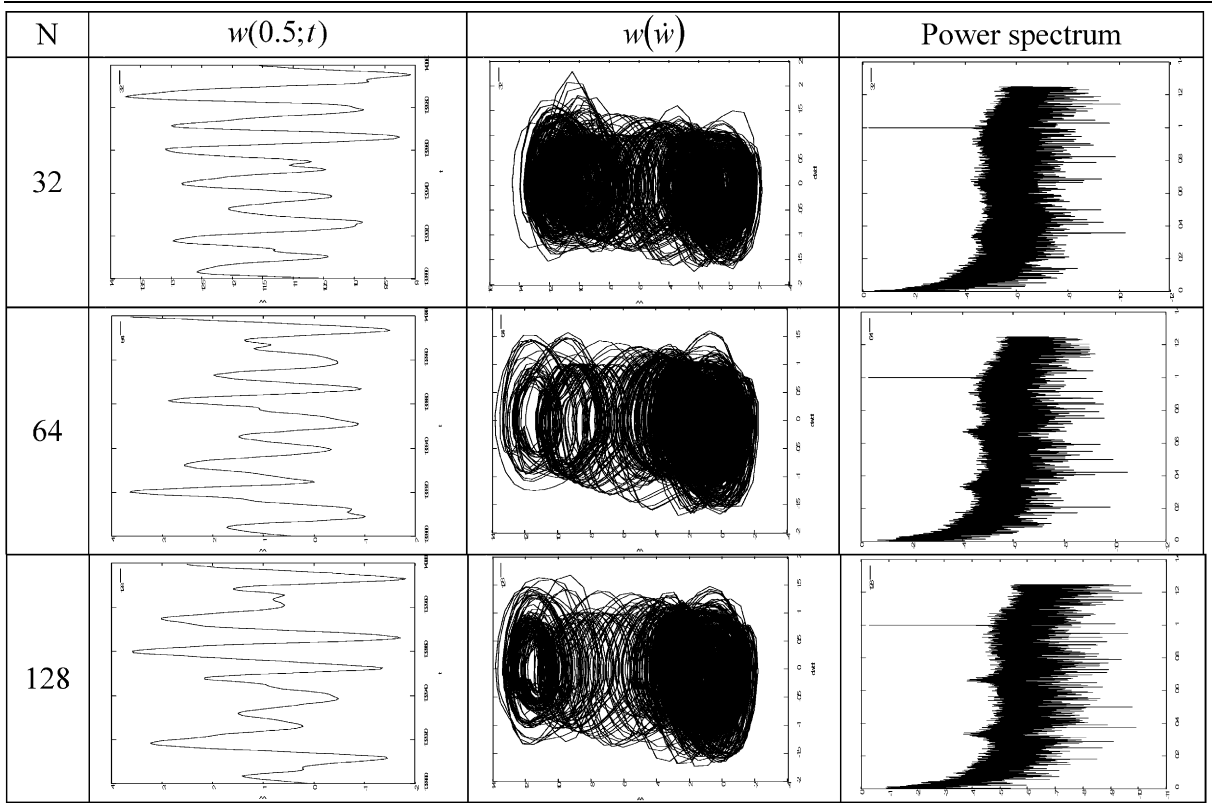
N	$w(0.5; t)$	$w(\dot{w})$	Power spectrum $S(\omega)$
16, 32, 64			

Table 2  
 Signals, phase portraits and power spectra (Section 3;  $q_0 = 3500$ )



has been developed by Benettin and other [1,17]. In this work, we follow the Benettin et al. approach.

As it has been mentioned already, Eq. (12) can be reduced to the following normal form:

$$\left\{ \begin{array}{l} \frac{du_i}{dt} = U_i, \\ \frac{dw_i}{dt} = W_i, \\ \frac{dU_i}{dt} = \Lambda_{x^2}(u_i) - \Lambda_x(w_i)(k_x - \Lambda_{x^2}(w_i)) + p(ih_1, t), \\ \frac{dW_i}{dt} = -\varepsilon W_i + \lambda^2 \left( -\frac{1}{12} \Lambda_{x^4}(w_i) + \Lambda_x(w_i)(\Lambda_{x^2}(u_i) - \Lambda_x(w_i)(k_x - \Lambda_{x^2}(w_i))) \right) \\ \quad + (\Lambda_{x^2}(w_i) + k_x)(\Lambda_x(u_i) - k_x w_i + 0.5(\Lambda_x(w_i))^2) + q(ih_1, t), \\ i = \overline{1, N-1}. \end{array} \right. \tag{16}$$



Fig. 1. Zones of periodicity, chaos and bifurcations in the  $\{q_0, \omega\}$  plane.

In order to compute all  $4(N - 1)$  Lyapunov exponents the following procedure is applied. First, an arbitrary orthonormal system of  $4(N - 1)$  vectors is chosen:

$$\{v_i^0, \|v_i^0\| = 1, (v_i^0, v_j^0) = \delta_{ij}, \quad i, 1 \leq j \leq 4(N - 1)\}. \quad (17)$$



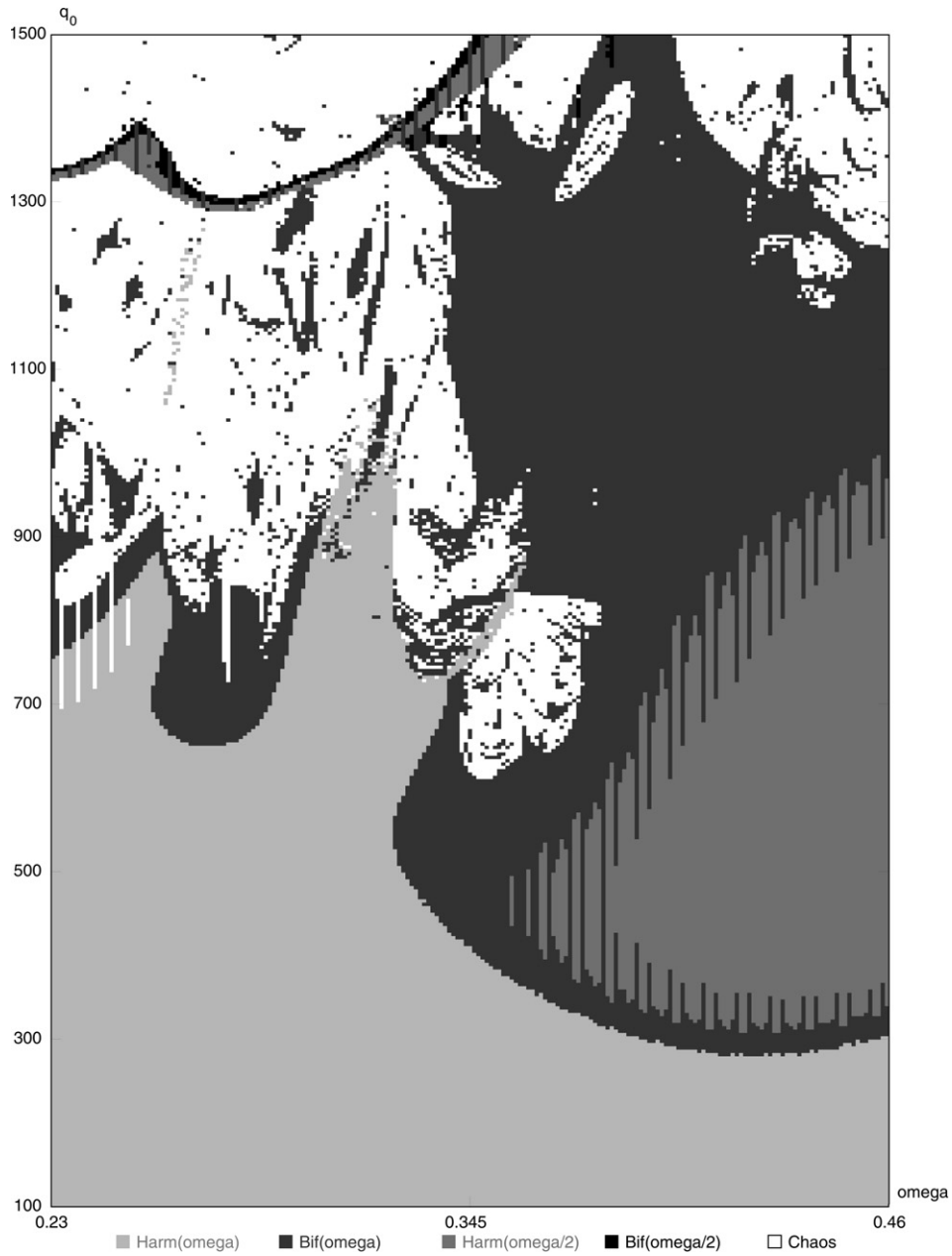


Fig. 2. The window from Fig. 1.

Let us, for simplicity, take the following system of equations:

$$\{(1, 0, \dots), (0, 1, 0, \dots), (0, 0, 1, \dots), \dots, (0, 0, 0, \dots, 1)\}.$$

Further, using a small computation step, a differential of the transformation defined by Eq. (17) (with respect to each of the vectors of system (18)) is computed along trajectory of the system. The vectors thus obtained  $\{\bar{v}_i^k, i = 1, 4(N-1)\}$  are normalized using the Gramm–Schmidt procedure:

$$\alpha_1^k = \|\bar{v}_1^k\|, \quad v_1^k = \frac{\bar{v}_1^k}{\alpha_1^k},$$

$$\alpha_i^k = \left\| \bar{v}_i^k - \sum_{j=1}^{i-1} (v_j^k, \bar{v}_i^k) v_j^k \right\|, \quad v_i^k = \frac{\bar{v}_i^k - \sum_{j=1}^{i-1} (v_j^k, \bar{v}_i^k) v_j^k}{\alpha_i^k}, \quad 1 \leq i \leq 4(N-1).$$

The Lyapunov exponents are defined through the formula

$$\lambda_i = \lim_{k \rightarrow \infty} \frac{1}{k \delta t} \sum_{j=1}^k \ln \alpha_i^j.$$

The problem of shell stability loss subject to a transversal sinusoidal load uniformly distributed on the shell surface, with excitation frequency equal to free vibration ones  $\omega_0 = 0.46$ , is further investigated.

The dependence  $w_{\max}(q_0)$  for the shell centre ( $x = 0.5$ , point A) and ( $x = 0.75$ , point B) is reported in Fig. 3. In the same figure, the characteristics  $\lambda_1(q_0)$  for the shell centre ( $x = 0.5$ , point A) is shown. Besides, in Fig. 3 in window E, the part of vibration character scale versus parameters  $q_0$  and  $\lambda_i(q_0)$  ( $i = 1, 2, 3$ ) is shown within the interval  $4000 \leq q_0 \leq 5000$ . In this figure, there are shown also zones *a*, *b*, *c*, *d*, *e*, and *f*. They will be analysed in more detail. In the interval  $0 \leq q_0 \leq 1247.3223$  harmonic vibrations with frequencies  $\omega_0$  and  $\omega_0/2$  are exhibited, and they undergo a series of bifurcations. For  $q_0 = 1247.3223$  two Hopf bifurcations have been detected (Table 3, where the same characteristics as in Table 2 are reported and the Poincaré section  $w_{t+T}(w_t)$ ). Increasing  $q_0$  by an amount of  $5 \times 10^{-5}$  pushes our mechanical system to chaos through Rayleigh–Takens–Newhouse scenario associated with frequencies generated by two Hopf bifurcations ( $q_0 = 1247.32235$ ). This description holds for a zone of transition from bifurcations to chaos (further referred as zone **a**). Owing to the theorem proved by Ruelle, Takens and Newhouse, chaos appears after two Hopf bifurcations and the system exhibits complex topology.

In zone **a**, a first-order jump in  $\lambda_1(q_0)$  occurs, and  $\lambda_1 > 0$ ,  $\lambda_2 < 0$ ,  $\lambda_3 < 0$ . A sudden increase of shell deflection is not observed. Further increase of  $q_0$  pushes our shell to a full chaotic state for  $q_0 = 1256$  (the signal  $w(t)$  is chaotic, and the power spectrum has a continuous fundamental part, whereas the phase portrait is entirely covered by trajectories). Variation of  $q_0$  by 0.615 ( $q_0 = 1256.615$ ) shifts the shell vibrations into an ordered chaotic state associated with a  $13T$  periodic motion ( $T$  is period of excitation), and the phase portrait and power spectrum are ordered. Here, a narrow window of bifurcations is observed ( $\lambda_i(q_0) < 0$ , ( $i = 1, 2, 3$ )). A further increase of  $q_0$  by 0.4 causes a Hopf bifurcation ( $q_0 = 1260$ ,  $\lambda_i(q_0) < 0$ , ( $i = 1, 2, 3$ )), and the so-called Sharkovsky order is reached at  $2 \cdot 13$  (see Section 6 of this work). Strange attractors begin to enlarge as may be seen by their Poincaré sections, and their numbers increase. For  $q_0 = 1260.5$ , i.e., increasing  $q_0$  by 0.5, the shell again exhibits a chaotic state associated with the last Hopf bifurcation (Sharkovsky order is of  $2 \cdot 13$ ). The phase portrait clearly shows a strange attractor, and its further development through observation of Poincaré sections ( $\lambda_1 > 0$ ,  $\lambda_2 < 0$ ,  $\lambda_3 < 0$ ). Then chaos successively turns into “full chaos”, i.e., the chaotic character of  $w(t)$  is clearly expressed, broadband phase portraits and power spectrum as for the case of  $q_0 = 1256$  ( $\lambda_1 > 0$ ,  $\lambda_2 < 0$ ,  $\lambda_3 < 0$ ) are

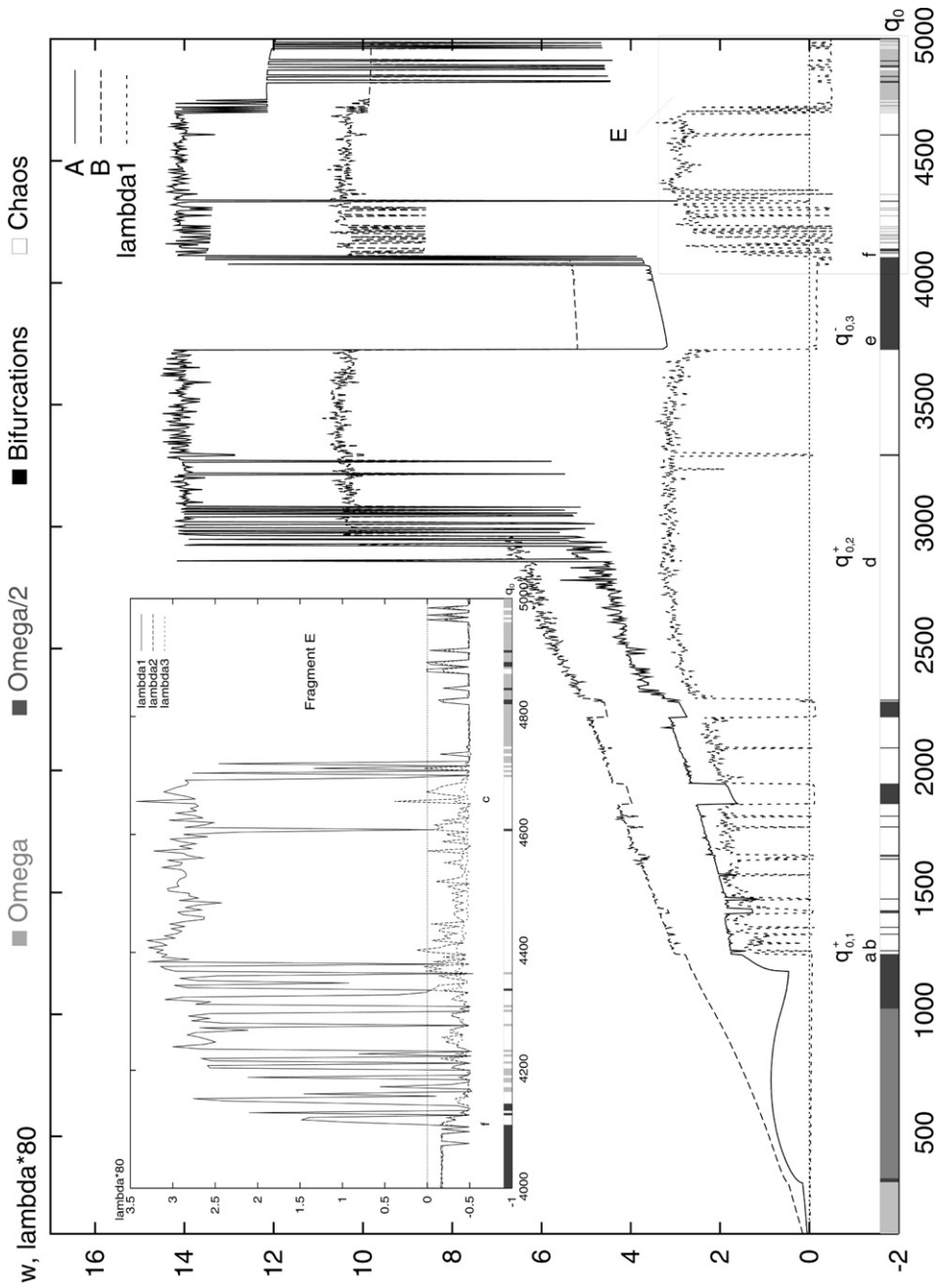
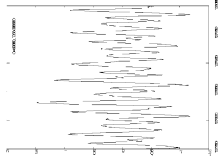
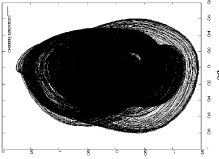
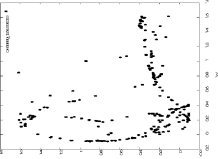
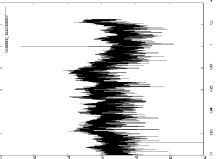
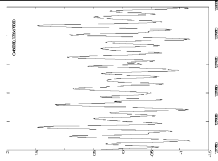
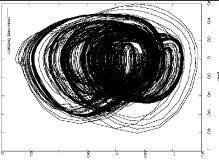
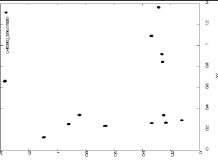
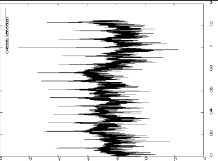
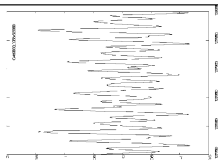
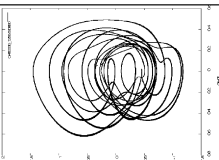
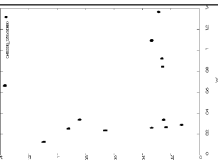
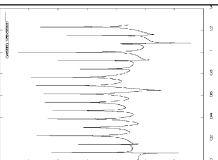
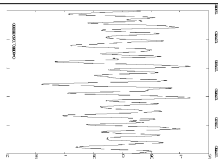
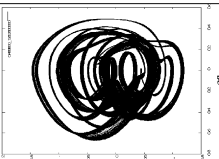
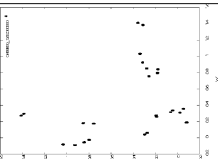
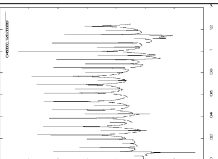
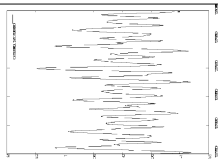
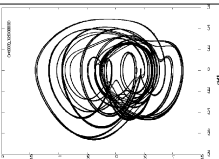
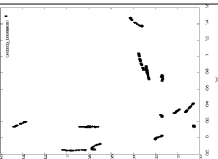
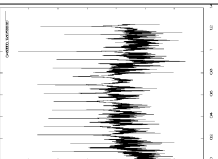
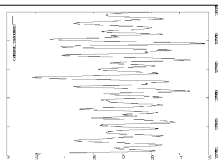
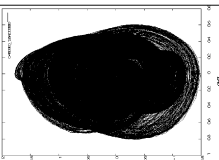
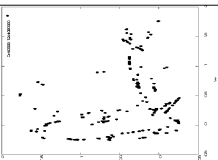
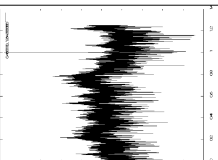


Fig. 3. Dependencies  $w_{\max}(q_0)$  and  $\lambda_i(q_0)$ ,  $i = 1, 2, 3$ .

Table 3  
 Signals, phase portraits, Poincaré sections and power spectra (Section 4)

Zone a, b			
$w(0.5;t)$	$w(\dot{w})$	$w_t(w_{t+T})$	$S(\omega)$
$q_0 = 1256, \lambda_1 > 0$			
			
$q_0 = 1256.615, \lambda_1 > 0$			
			
$q_0 = 1256.62, \lambda_1 < 0$			
			
$q_0 = 1260, \lambda_1 < 0$			
			
$q_0 = 1260.5, \lambda_1 > 0$			
			
$q_0 = 1264, \lambda_1 > 0$			
			

exhibited. The behaviour described is related to zone **b** (see Table 3). The value of maximal deflection in zones “**a**” and “**b**” is practically the same, i.e., a sharp deflection increase is not observed, compared with what we usually observe during a static stability loss. The value of  $q_{0,1}^+ = 1256$  is referred to below as first dynamic critical load.

## 5. “Chaos–hyperchaos” phase transitions

In what follows we analyse an evolution of a vibrational process with increase of the amplitude of excitation. It is worth noting that the problem of attractor evolution with increase of  $q_0$ , within a chaotic state, is rather rarely investigated (even in the problems of radiophysics and electronics). One may expect the development of a chaotic set, the occurrence of continuous power spectrum and/or synchronization processes. It has been already shown that qualitative changes in chaos structure can already be observed in systems with 11/2 degrees of freedom [11]. It is shown in the theory of shells analysis that “chaos–chaos” transition does not allow for bifurcations in chaos to be matched with an increase of the Lyapunov dimension of attractor  $D_L$ . Owing to the definition, the Lyapunov dimension is computed through the Lyapunov spectrum of exponents (LSE). However, there is not any unique link between Lyapunov exponents and attractor dimension (AD).

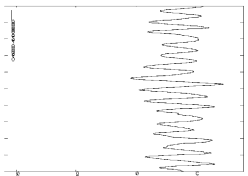
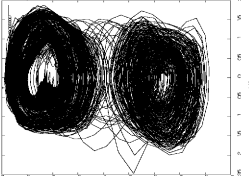
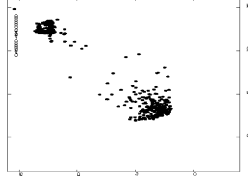
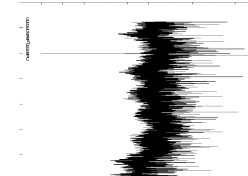
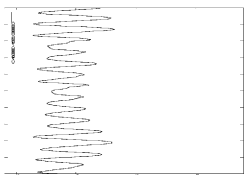
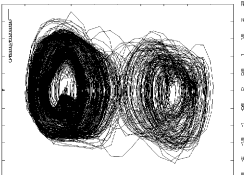
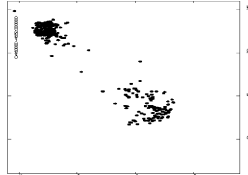
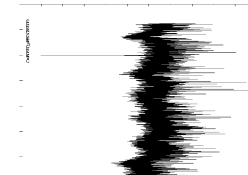
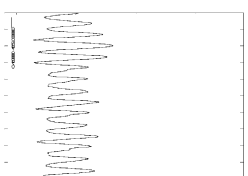
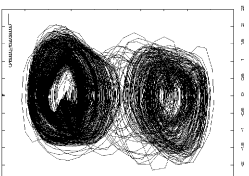
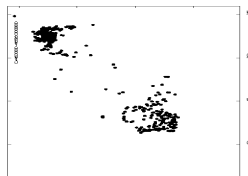
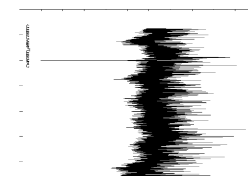
Intuitively, an occurrence of qualitative changes of physical characteristics of an attractor associated with an occurrence of positive Lyapunov exponent is more evident, than analogous changes during an increase of Lyapunov dimension of an integer number. Indeed, in a case of occurrence of additional positive Lyapunov exponent a new unstable direction associated with the system trajectory occurs. It causes qualitative changes of system dynamics, which is manifested by physical characteristics. On the other hand, the Lyapunov dimension defines a dimension of an averaged local volume preserving its magnitude, i.e., it is not compressing and not expanding.

Positive, zero and negative exponents are responsible for Lyapunov’s dimension. The latter ones are responsible for stability type of the motion, but they do not influence steady-state motions. They influence rather metrical attractor properties. For instance, it has been shown elsewhere that in the general case it is impossible to extract negative Lyapunov exponents from experimental data.

In what follows we study transition within chaos during a change of the Lyapunov spectrum, as well transitions from strange attractor with one positive exponent into hyperchaos, i.e., chaos with two positive exponents. Further, this transition will be referred as the “chaos–hyperchaos” scenario.

In Table 4, the dependencies  $w(t)$ ,  $w(\dot{w})$ , Poincaré section  $w_i(w_{i+T})$  and power spectrum for the central shell point subjected to external load  $q_0 \sin 0.46t$  are reported. The stated characteristics are given for the values of the parameters characterising intensity of the external load:  $q_0^{(1)} = 4648$ ,  $q_0^{(2)} = 4652$  and  $q_0^{(3)} = 4656$  (see also LSE ( $q_0$ ) in Fig. 3). For  $q_0^1$ :  $\lambda_1 > 0$ ,  $\lambda_2 < 0$ ,  $q_0^2$ :  $\lambda_1 > 0$ ,  $\lambda_2 > 0$ ,  $q_0^3$ :  $\lambda_1 > 0$ ,  $\lambda_2 < 0$ , i.e., there exist three state of the system. For  $q_0^1$  and  $q_0^3$  the system is in chaotic state, for  $q_0^2$  it is in “chaos–hyperchaos” state. The dynamical system associated with  $q_0^1$  and  $q_0^3$  has two chaotic attractors lying in the corners of Poincaré diagonal, whereas for  $q_0^2$  matching of these attractors in the centre  $w_i(w_{i+T})$  of the space occurs. In the “chaos–hyperchaos”  $\lambda_1$  and  $\lambda_2$  achieve their maximal positive values, whereas  $\lambda_3$  practically has not been changed, remaining in negative space.

Table 4  
Signals, phase portraits, Poincaré sections and power spectra (Section 5)

$q_0$	$w(0.5;t)$	$w(w)$	$w_t(w_{t+T})$	Power spectrum $S(\omega)$
Chaos (4648)				
Hyper-chaos (4652)				
Chaos (4656)				

### 6. Sharkovsky’s type periodicity for differential equations of Vlasov–Marguerre shells

Feigenbaum began his investigation studying intervals between period doubling bifurcations exhibited by a logistic map. This map occurred during considerations of ecosystems and was first analysed by Ferhulst in 1845, and it is often known as Ferhulst diagram  $y = x^2 + c$ . Feigenbaum discovered a universal property of this map. The period doubling route to chaos detected by him occurs not only during iterations of the map  $cx(1 - x)$ , but also in a case of wide class of mapping of an interval into itself, like  $x^2 + c$ ,  $c \sin(\pi x)$  and  $cx^2 \sin \pi x$  defined on suitable intervals.

An orbit diagram presented in Fig. 4 represents attracting periodic orbits for the functions of the form  $f_c(x) = x^2 + c$ . It is worth noting that in some intervals, the diagram is interrupted. For instance, for  $c \approx 1.75$  a white zone is visible and attracting orbits have period 3. A natural question arises: Do any other periodic orbits exist? These orbits should be repellers, since on the diagram we see only attracting orbits. In fact, an occurrence of orbits with period 3 is matched with occurrence of orbits with periods  $n = 1, 2, 3, \dots$

An interesting property of the orbits with period 3 has been considered by Li and Yorke [18] in 1975, but it occurred that the results became a particular case of Sharkovsky theorem published in 1964.

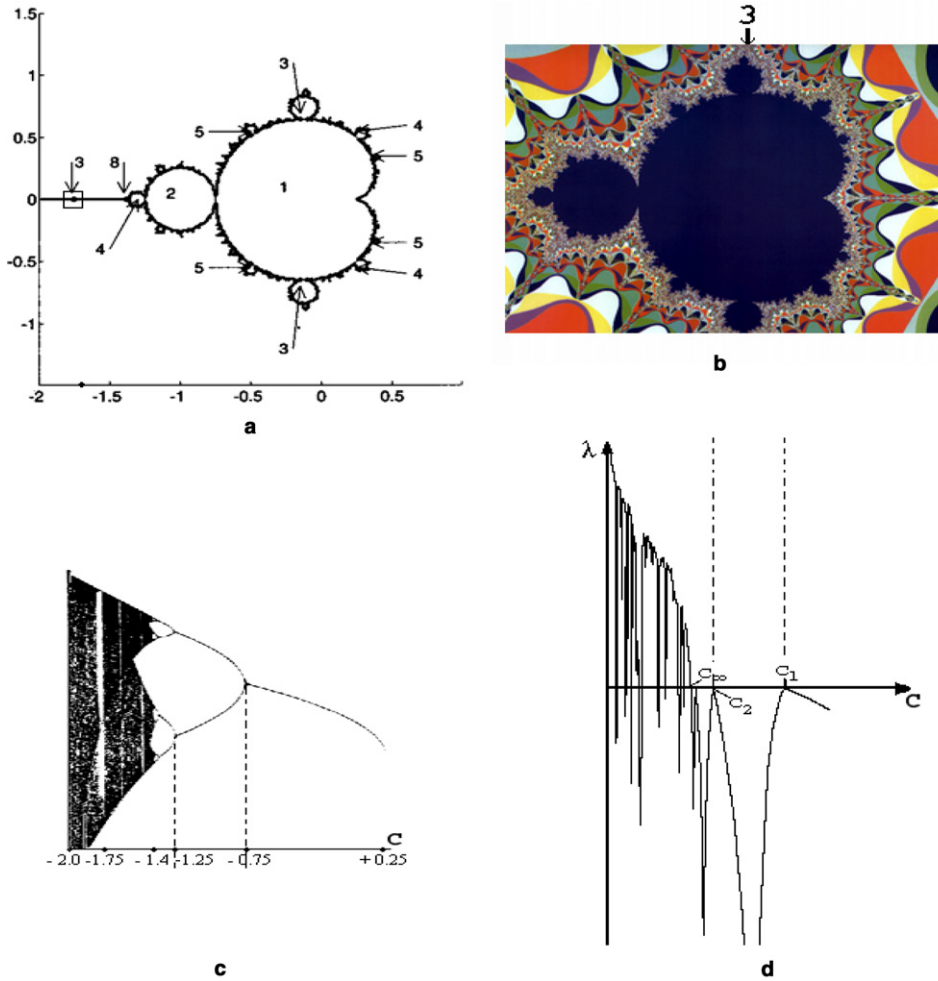


Fig. 4. Characteristics of the Mandelbrot sets: periods of maps  $f_c(z) = z^2 + c$  (a); window of 3-periodicity (b); bifurcation free for  $f_c(x) = x^2 + c$  (c); Lyapunov exponent for  $f_c(x) = x^2 + c$  (d).

**Theorem** (Sharkovsky, [19]). *Let  $I$  be finite or infinite interval in  $\mathbf{R}$ . Assume that mapping  $f: Z \rightarrow I$  is continuous. If there exists a point  $f$  of period  $n$ , then there is also a point  $f$  of period  $k$  for every integer positive  $k, k > n$ , taken from the following Sharkovsky's order series*

- 3, 5, 7, 9, ...
- $2 \cdot 3, 2 \cdot 5, 2 \cdot 7, 2 \cdot 9, \dots$
- $2^2 \cdot 3, 2^2 \cdot 5, 2^2 \cdot 7, 2^2 \cdot 9, \dots$
- $2^3 \cdot 3, 2^3 \cdot 5, 2^3 \cdot 7, 2^3 \cdot 9, \dots$
- .....
- ..... $2^n, \dots, 2^2, 2^1, 1$

Let us compare transformations  $f_c(x) = x^2 + c$  and  $f_c(z) = z^2 + c$ , i.e., logistic transformations in the real and complex plane, and the associated Lyapunov exponent  $\lambda_1(c)$  constructed for  $f_c(x) = x^2 + c$  (Fig. 4). Diagrams of the orbits for two functions possess attracting, repelling and neutral points, which correspond to stable, unstable and neutral equilibrium states.

Recall that if one starts in the neighbourhood of fixed point, to which successive iterations will be closer and closer, then the fixed point is called attractor. In contrast, if one starts in the neighbourhood of fixed point from which successive iterations will go away, then the fixed point is called repeller. A neutral fixed point possesses the following property: starting in its vicinity and always remaining on it.

In order to define a fixed point  $\bar{z}$  of the map  $f(z)$  one should compute  $f'(z)$ . Namely, if  $|f'(\bar{z})| < 1$ , then  $\bar{z}$  is called attractor; if  $|f'(\bar{z})| > 1$ , then  $\bar{z}$  is called repeller; if  $|f'(\bar{z})| = 1$ , then the fixed point is neutral.

For the rational mapping, owing to Sharkovsky's theorem, there exist cycles of all orders  $n = 2, 3, 4, \dots$

An attractor in a complex plane is a point to which the following iterational process  $z_{n+1} = f(z_n)$ ,  $n \rightarrow \infty$  is convergent. Sometimes there are a few such attractors, which may consist of an infinitely numerous set of points or create a continuous curve, or any other, say, Cantor type set.

The Mandelbrot set ( $M$ ) in the complex plane is shown in Fig. 4. Any complex number  $c$  either belongs to the Mandelbrot set or not. In Fig. 4 periods of the Mandelbrot set (Fig. 4a), bifurcations diagrams of the orbits of  $f_c(x) = x^2 + c$  (Fig. 4c),  $\lambda_1(c)$  (Fig. 4d) and a window of Mandelbrot set in vicinity of the point  $c = -1.75 + 0i$  (Fig. 4b) are reported, respectively. The value  $c = -0.481762 - 0.531657i$  corresponds to stable period 5 limit cycle, i.e., parabolic-type dynamics occurs. For  $f_c(x) = x^2 + c$ , in vicinity of  $c \approx 1.75$ , a white zone is visible and attracting orbit has period 3. In this zone,  $\lambda_1 < 0$ . Points  $c_1$  and  $c_2$ , where  $\lambda_1 = 0$ , correspond to bifurcation points, and the values of  $c$  for  $f_c(z)$  and  $f_c(x)$  are approximately the same. The value of  $c$ , for which attracting periodic points of period 2 in Julia set exist, lie inside the circle  $|c + 1| = 1/4$  ( $c_1 = -3/4$ ,  $c_2 = -5/4$ ). For almost the same values ( $c_2 \leq c \leq c_1$ ) there exist attracting points of period 2 of the function  $f_c(x)$ . In other words, the diagram  $f_c(x)$  characterizes a behaviour on a real axis of the Mandelbrot set.

The boundary of attracting points is defined through a cardioid, and the attracting points lie inside of it. Since the cardioid belongs to the  $x$ -axis for  $c \in [-3/4, 1/4]$ , this is associated with the part of the orbital diagram, where only one branch exists.

In what follows we are going to study how the Sharkovsky's theorem relates to the periodic orbits of the Marguerre–Vlasov differential equations (5) and (6) with  $k_x = 48$ ,  $\varepsilon = 0.01$  subject to a transversal load  $q = q_0 \sin \omega_0 t$  (simple ball-type support along shell contour (7) and zero values initial conditions are applied). Elastic, homogeneous and isotropic material is taken  $\nu = 0.3$ ; excitation frequency is equal to the frequency of linear plate vibrations  $\omega_0 = 0.46$ . Signals in both shell centre and its quadrant, power spectra and Poincaré maps for the orbits associated with Sharkovsky's theorem are reported.

Sharkovsky's series of the form 3, 5, 7, 9, 11, 13 (Table 5),  $2 \cdot 3$ ,  $2 \cdot 5$ ,  $2 \cdot 7$ ,  $2 \cdot 9$ ,  $2 \cdot 11$ ,  $2 \cdot 13$  (Table 6) and  $2^1$ ,  $2^2$ ,  $2^3$ ,  $2^4$ ,  $2^5$ ,  $2^6$  (Table 7) are shown. Besides the (given in previous tables) dependencies  $w(0.5;t)$ ,  $w(\dot{w})$ ,  $w_t(w_{t+T})$  and  $S(w)$ , in Tables 5–7 modal characteristics  $w(\partial w/\partial x)$  for the



**Table 5**  
 Dynamical characteristics (Sharkovsky's series 3, 5, 7, 9, 11, 13)

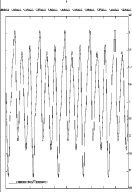
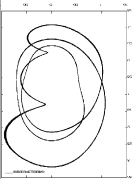
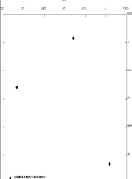
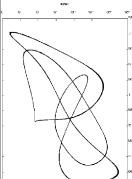
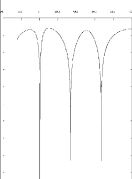
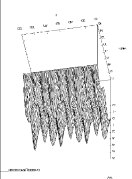
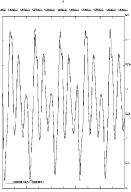
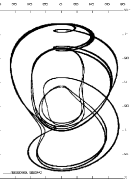
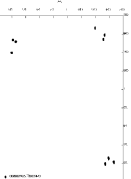
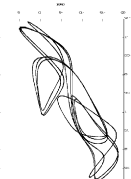
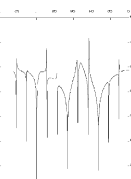
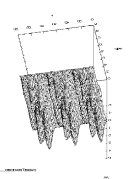
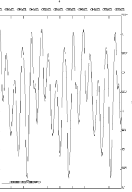
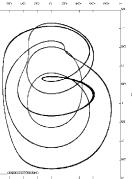
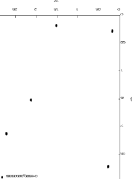
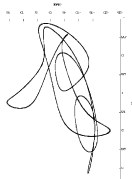
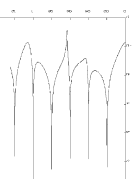
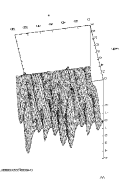
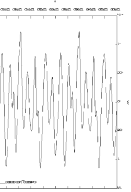
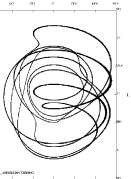
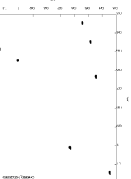
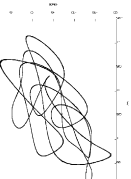
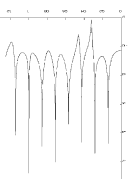
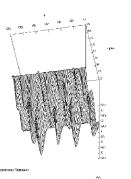
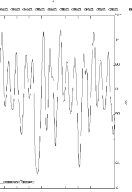
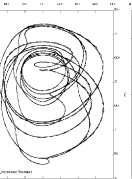
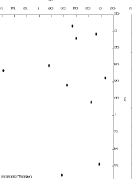

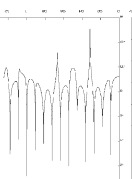
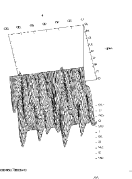
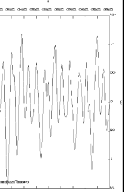
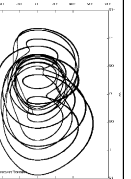
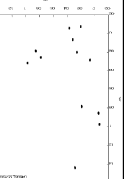

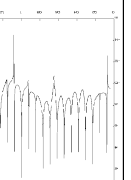
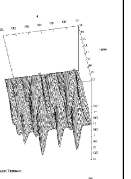
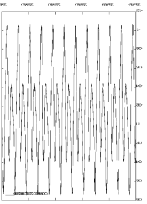
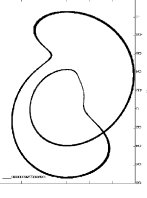
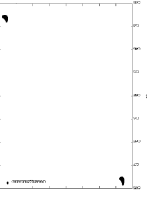

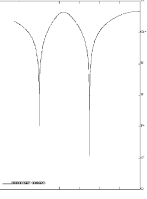
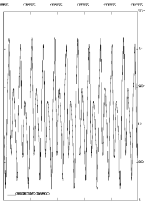
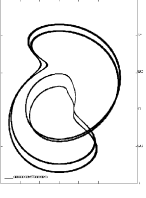
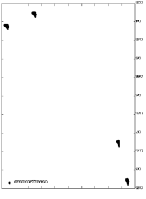
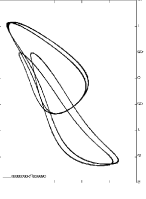
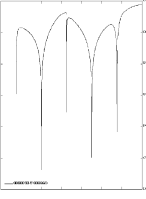
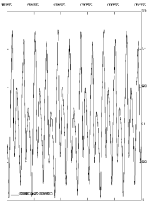
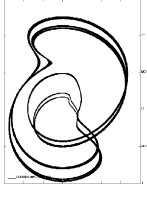
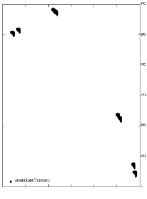
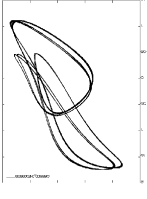
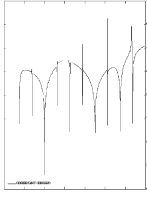
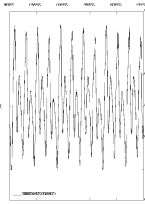
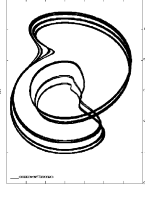
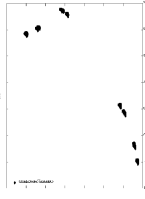
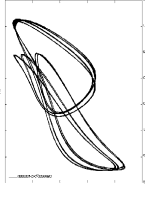
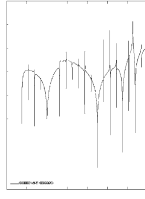
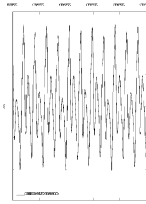
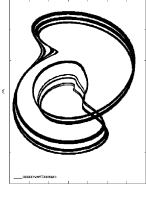
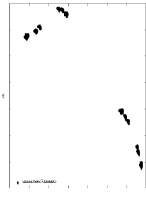
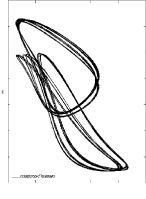
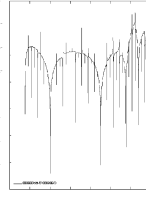
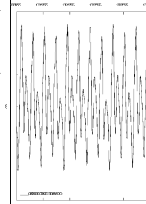
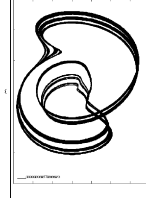
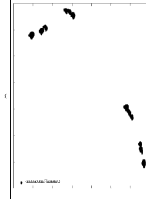
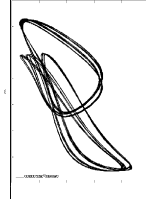
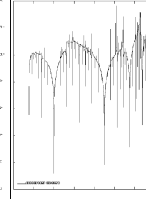
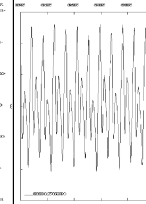
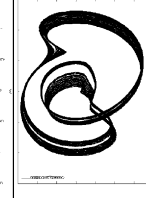
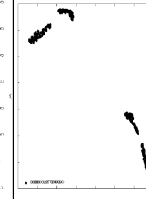
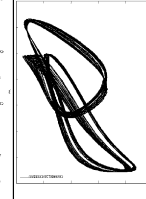
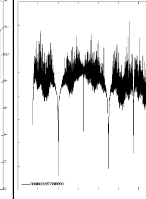
$w(0.5; t)$	$w(w)$	$w_i(w_{i+T})$	$w(\partial w / \partial x)$	$S(\omega)$	Surface	SE/ $q_0$
						3 / 3740
						3*3 / 1936
						5 / 2220
						7 / 1472
						11 / 1328
						13 / 1257

Table 6  
 Dynamical characteristics (Sharkovsky's series  $2 \cdot 3, 2 \cdot 5, 2 \cdot 7, 2 \cdot 9, 2 \cdot 11, 2 \cdot 13$ )

$w(0.5;t)$	$w(w)$	$w_i(w_{i-1})$	$w(\partial w / \partial t)$	$S(\omega)$	Surface	$SE/q_0$
						2*3 / 3728
						2*3*3 / 1945
						2*5 / 1420
						2*7 / 1636
						2*11 / 1280
						2*13 / 1260

Table 7  
 Dynamical characteristics (Sharkovsky's series  $2^1, 2^2, 2^3, 2^4, 2^5, 2^6$ )

$w(0.5; t)$	$w(\psi)$	$w_i(w_{i+r})$	$w(\partial w / \partial x)$	$S(\omega)$	SE/ $q_0$
					2 / 2350
					$2^2$ / 2400
					$2^3$ / 2470
					$2^4$ / 2494
					$2^5$ / 2499
					$2^6$ / 2500
					Chaos / 2510

shell point  $x = 0.375$ , surfaces and Sharkovsky's exponents (SE) for the corresponding  $q_0$  are given. It should be noted that the given Sharkovsky series do not appear in a sequence in our continuous system, but they are located in the whole space of the control parameters  $\{q_0, \omega_0\}$  (Figs. 1, 2). The following properties have been detected:

1. During a period 3 tripling bifurcation, a partition of the fundamental signal into 3(5) equal parts is observed. In the associated Poincaré section 3, 5, 7, 9, 11, and 13 points are observed. For the series  $2 \cdot 3, 2 \cdot 5, 2 \cdot 7, 2 \cdot 9, 2 \cdot 11, 2 \cdot 13$  groups of doubled points are observed. In the phase portraits period doubling of periodic orbits is exhibited. Furthermore, the Poincaré map points distribution is ordered for orbits with periods 3;  $2 \cdot 3$ ; 9;  $2 \cdot 9$ ; 13;  $2 \cdot 13$ , whereas for the series 5, 7, 11 and  $2 \cdot 5, 2 \cdot 7, 2 \cdot 11$  they are destroyed and lie in the phase plane in an arbitrary manner. The given orbits are windows of periodicity in an ocean of chaos, and their structure is the same in whole range of the control parameters  $\{q_0, \omega_q\}$  (Fig. 4). All windows of periodicity possess negative Lyapunov exponents  $\lambda_i < 0, i = 1, 2, 3$ .
2. For each of the orbits discussed in item 1, changes of shell deflections in time  $w(x, t)$  ( $0 \leq x \leq 1; 127,500 \leq t \leq 128,000$ ) are given in Table 6. It allows analyzing shell deformation with respect to a type of a considered orbit. Owing to an increase of the period, deflections exhibit deeper chaotic dynamics, i.e., a transition into spatial chaos is observed.

## 7. Vibrations of cylindrical panels in zones “d”, “e”, and “f”

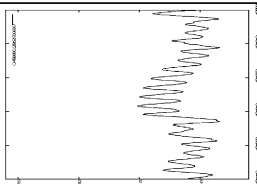
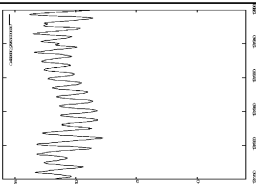
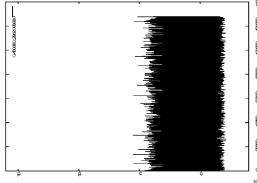
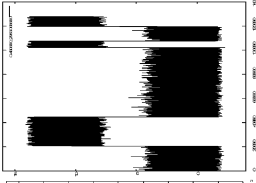
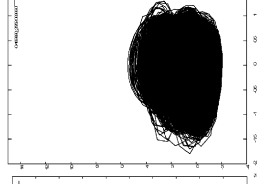
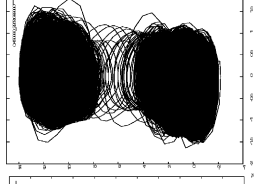
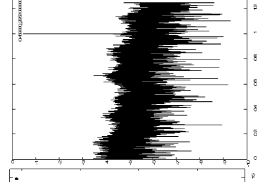
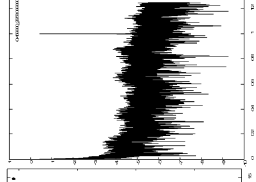
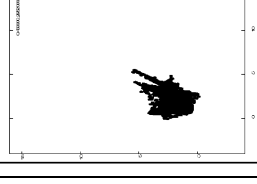
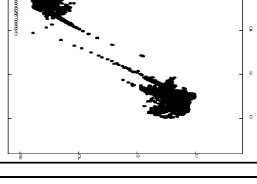
In order to fully understand nonlinear vibrations of our analysed panels, their dynamics in zones “d”, “e”, “f” is studied (Table 8–10, respectively).

The given zones are extracted from a general picture of vibrations. For instance, in zone “d” associated with chaos a fast panel deflection is observed, i.e., a second dynamical stability loss for  $\lambda_1 > 0, q_{0,2}^+ = 2953$  appears.

In Table 8, power spectrum, phase portraits, signals  $w_A(t)$ , points of the signals c and d, and the Poincaré map for pre-critical ( $q_0 = 2952$ ) and critical ( $q_{0,2}^+ = 2953$ ) states are reported. The given characteristics show vibrations as chaotic ones, and for  $q_{0,2}^+$ , the phenomenon of convexity–concavity is observed. It is worth noting that attractors corresponding to convexity–concavity exhibit mirror-type reflection. Let us further analyse vibrations in zones “e” and “f”, i.e., a transition of our system from chaos into a periodic window, and then an exit from this window.

In Table 9, the same characteristics as in Table 8, but for the points  $q_0 = 3724$  (chaotic zone) and  $q_0 = 3724.5$  (bifurcation zone) are reported. For  $q_0 = 3724$  a full chaotic state is observed, and the series of convexity–concavity appears successively, and two chaotic attractors are matched in the Poincaré sections. Here, so-called intermittency is exhibited. A variation of the amplitude of excitation by 0.5 pushes our system into Sharkovsky bifurcation state of the type  $2 \cdot 3$ . Then, a collapse of the chaotic attractor, and creation of 3 groups of doubled points associated with a previous period tripling and Hopf bifurcations occurs. In Table 10, analogous characteristics for zone “f”, i.e., an exit from the bifurcation zone, are shown. For  $q_0 = 4108.5$  complex vibrations of the system owing to the ordered series due to Sharkovsky's series 3;  $2 \cdot 3$ , and occurrence of a new independent frequency, are observed. An increase of  $q_0$  on amount of

**Table 8**  
**Dynamical characteristics (zone d)**

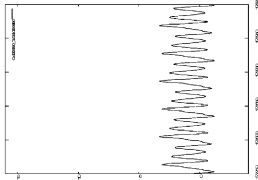
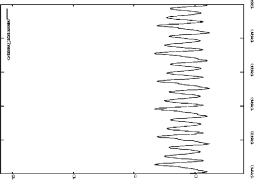
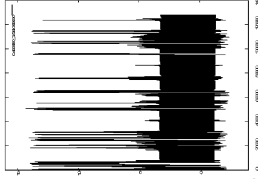
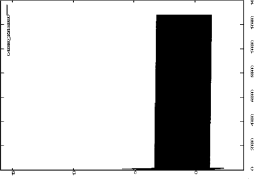
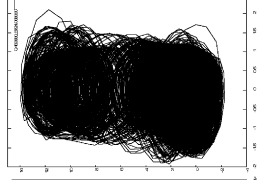
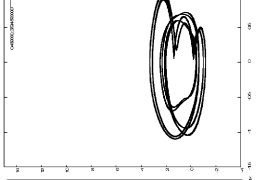
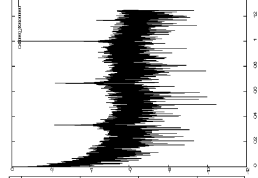
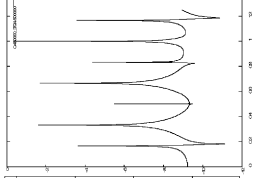
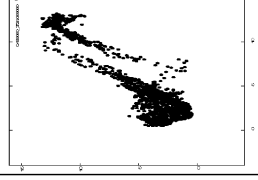
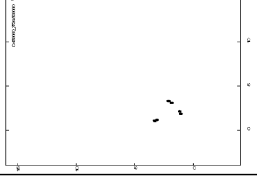
Zone d		
	$q_0 = 2952$	$q_0 = 2953$
$w(t), t \in [127750, 128000]$		
$w(t), t \in [0, 128000]$		
$w(\dot{w})$		
$S(w)$		
$w_t(w_{t+T})$		

0.5 pushes the system to new bifurcation, i.e., concavity occurs, and the system vibrates with fundamental frequency and frequency generated through the Hopf bifurcation. Further increase of  $q_0$  on amount of 0.5 suddenly transforms the system into chaos similar to that of zone “e”.

### 8. Computation of a Feigenbaum constant

In the analysed cylindrical infinitely length panel subjected to transversal sinusoidal load there are zones where a transition from harmonic to chaotic vibrations takes place owing to the

Table 9  
Dynamical characteristics (zone e)

Zone e		
	$q_0 = 3724$	$q_0 = 3724.5$
$w(t), t \in [127750, 128000]$		
$w(t), t \in [0, 128000]$		
$w(\dot{w})$		
$S(w)$		
$w_t(w_{t+T})$		

Feigenbaum scenario [20], i.e., a series of successive Andronov–Hopf bifurcations appear. In computational experiments, the series  $\{q_0\}$  of period doubling bifurcation of the period 7 orbit occurred, yielding a possibility to compute the Feigenbaum constant (Table 11).

Analysis of the results included in Table 11 shows that a good convergence for the series  $\{q_0\}$  for the computation of the Feigenbaum constant holds for six Hopf bifurcations. Further increase of the load amplitude causes difficulties in the computation of successive bifurcations, since accuracy of computations is decreased.

Table 10  
Dynamical characteristics (zone f)

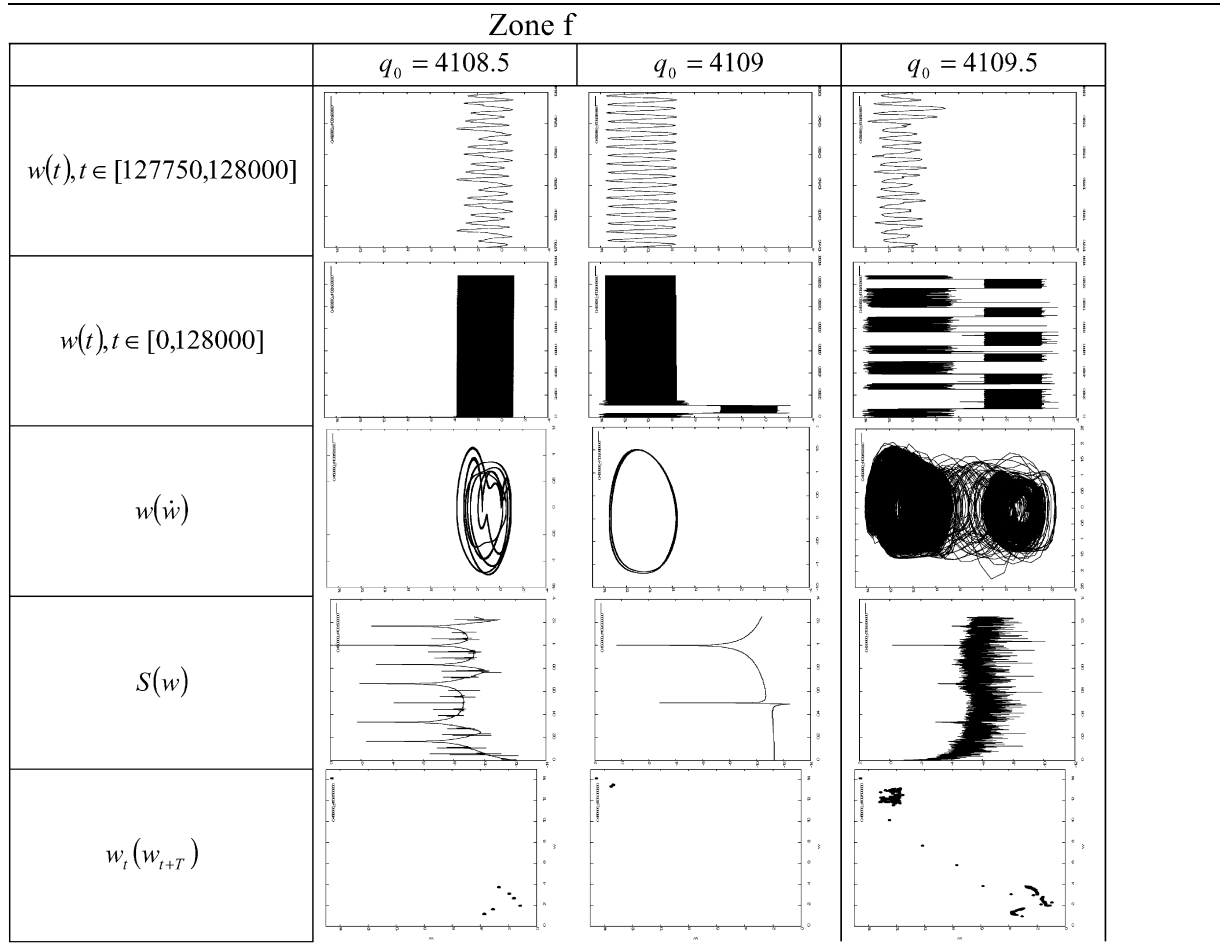


Table 11  
Computation of the Feigenbaum constant

No. of bifurcation	$q_0$	Feigenbaum constant
1	2287.70123873	
2	2371.12397775	
3	2464.88647395	0.889724
4	2492.97413230	3.338210
5	2498.67513981	4.926788
6	2499.89796544	4.662159
7	2500.16165971	4.637286

## 9. Conclusions

Analysis of complex vibrations of cylindrical panel with  $k_x = 48$  shows that in the space of control parameters  $\{q, \omega_p\}$  there exist subspaces, where a transition into chaos is realized through classical Feigenbaum and Ruell–Takens–Newhouse scenarios.

The finite difference method has been applied in order to reduce our continuous deformable system to the consideration of a set of ordinary differential equations. Poincaré maps, pseudomaps, power spectra and Lyapunov exponents have been applied to consider the chaotic vibrations of flexible infinite length cylindrical panels.

## References

- [1] Lorenz EN. Deterministic nonperiodic flow. *Atmos Sci* 1962;20(1):130–41.
- [2] Abe A, Kobayashi Y, Yamada G. Two-mode response of simply supported, rectangular laminated plates. *Int J Non-Linear Mech* 1998;33(4):675–90.
- [3] Nayfeh TA, Vakakis AF. Subharmonic traveling waves in a geometrically non-linear circular plate. *Int J Non-Linear Mech* 1994;29(2):233–45.
- [4] Wei-Zhang, Zhaomiao L, Pei Y. Global dynamics of a parametrically and externally excited thin plate. *Nonlinear Dyn* 2001;24:245–68.
- [5] Arafat HN, Nayfeh AH. Modal interactions in a thermally loaded annular plate. In: *Proceedings of DETC'03 of ASME design engineering technical conferences*, 2–6 September 2003, Chicago, Illinois, USA, p. 11 (CD Rom).
- [6] Biswas P, Kapoor P. Non-linear vibrations of circular plates at elevated temperature. *Proceedings of fourth int. conf. on numerical methods in thermal problems*, Part 2, Swansea, UK, 15–18 July 1985. p. 1493–1501.
- [7] Li S-R, Zhou Y-H, Song X. Non-linear vibration and thermal buckling of an orthotropic annular plate with a centric rigid mass. *J Sound Vibr* 2002;251:141–52.
- [8] Lasiecka I. Finite dimensionality and compactness of attractors for von Kármán equations with nonlinear dissipation. *Nonlinear Diff Equat Appl* 1999;6:437–72.
- [9] Krysko VA, Awrejcewicz J, Bruk V. On the solution of a coupled thermo-mechanical problem for non-homogeneous Timoshenko-type shells. *J Math Anal Appl* 2002;273(2):409–16.
- [10] Krysko VA, Awrejcewicz J, Bruk V. On existence and uniqueness of solution to coupled thermomechanics problem of non-homogenous isotropic plates. *J Appl Anal* 2002;8(1):129–39.
- [11] Awrejcewicz J, Krysko VA. *Nonclassic thermoelastic problems in nonlinear dynamics of shells*. Berlin: Springer; 2002.
- [12] Awrejcewicz J, Krysko VA, Krysko AV. Spatio-temporal chaos and solitons exhibited by von Kármán mode. *Int J Bifurcat Chaos* 2002;12(7):1465–513.
- [13] Awrejcewicz J, Krysko VA, Narkaitis GG. Bifurcations of a thin plate-strip excited transversally and axially. *Nonlinear Dyn* 2003;3:187–209.
- [14] Awrejcewicz J, Krysko VA, Krysko AV. Complex parametric vibrations of flexible rectangular plates. *Meccanica* 2004;39(3):221–44.
- [15] Awrejcewicz J, Krysko VA, Narkaitis GG. Nonlinear vibration and characteristics of flexible plate-strips with non-symmetric boundary conditions. *Commun Nonlinear Sci Numer Simulat* 2006;11(1):95–124.
- [16] Awrejcewicz J, Krysko VA. On the vibration of the Euler–Bernoulli beam with clamped ends deflection constraints. *Int J Bifurcat Chaos* 2005;15(3) [special issue] (available online in September 2005).
- [17] Zaslavsky GM, Chirikov BV. Stochastic instability of nonlinear oscillations. *Uspiekhii Fiz Nauk* 1971;105(1):3–29.
- [18] Li TY, Yorke JA. Period three implies chaos. *Am Math Monthly* 1975;82:985–92.
- [19] Sharkovsky AN. Coexistence of cycles of a continuous map of a linear into itself. *Ukr Math Z* 1964;16(1):61–71 [in Russian].
- [20] Feigenbaum MJ. The universal metric properties of nonlinear transformations. *J Stat Phys* 1979;21(6):689–706.